

Applications of Computational Geometry for Automatic Transformation to Unstructured Reservoir Gridding

Firas H. Melaih, Dr. Ali A. Al-Turki, Razen M. Al-Harbi, and Majdi A. Baddourah

Abstract /

Reservoir simulation is becoming a standard practice for oil and gas companies, helping with decision making, reducing reservoir characterization uncertainties, and better managing hydrocarbon resources. The reservoir model sizes can reach multibillion grid cells, which led Saudi Aramco to develop an in-house massively parallel reservoir simulator, as well as a pre- and post-reservoir simulation environment¹. Compared to structured grid modeling, unstructured grid modeling and billion cell pre- and post-simulation processing of reservoir simulation provides engineers with advanced modeling capabilities to represent complex well geometries and near wellbore modeling. Mapping between structured and unstructured (2.5D) domains is not a straightforward task. The indexing in unstructured grids makes creating property modifiers, conducting near wellbore modeling, and local grid refinement difficult.

We present a developed workflow to automatically transform the modeling of property modifiers, near wellbore modeling and local grid refinement between the structured and unstructured domains. Several computational geometry algorithms were developed for efficiency and accuracy, which will preprocess the corners of the top layer cells into data structures. To map regions of interest between domains, the algorithms find all corner points inside them. The regions are translated using the algorithms and the results are exported in the unstructured format.

The two challenges are that the number of corner points is massive, therefore, a brute-force search — even for a simple region of interest is expensive — and irregular regions of interests result in very costly search complexity. We address these by preprocessing the input data in the form of range trees. We also propose a free-shape polygonal search strategy to find all corner points in the regions of interest.

The range tree algorithm provided a fast and robust workflow to perform the transformation from structured to unstructured gridding domains, while providing ease of use with a visual component, to aid with property transformation, near wellbore modeling, and local grid refinement. The algorithm's performance was measured using the time complexity of the preprocessing time, query time, and the space complexity.

The range tree approach is first compared to the other approaches, requiring only $O(\log(n)+k)$ operations, compared to the $O(n)$ of linear search. It takes a costly $O(n\log(n))$ time to preprocess the data into the range tree, however, that is a one-time cost, as well as requiring $O(n\log(n))$ space in memory.

This work is a major milestone to promote and support the unstructured grid modeling approach for large- and small-scale reservoir simulation models. The algorithm will provide engineers with a simplified workflow and smooth transitioning, allowing advanced capabilities to model complex well geometries and near wellbore modeling, while preserving complex geological features. In addition, this algorithm provides the building blocks in facilitating the migration and conversion of existing structured simulation models.

Introduction

Reservoir simulation is one of the commonly used tools in the oil and gas industry to estimate recovery and conduct studies to support strategic decisions. It is effectively used for the development, production optimization, and management of oil fields. This simulation also gives the reservoir engineers the ability to assess multiple production scenarios to maximize oil recovery and minimize operational cost.

To solve for finite-difference fluid flow (oil, gas, and water) equations for hydrocarbon-bearing formations, a geological model is built from different sources of data sources characterizing the formations. A dynamic model is then built by integrating the static geological model with field dynamic data — pressure, fluid rates, and properties, and development strategies.

The reservoir model needs to be discretized into smaller units to solve fluid flow equations to calibrate and history

match historical field data, and perform predictions. The process of discretization is called “gridding,” and the resulting discretized model is referred to as a “numerical grid.” The complexity of the reservoir model grid discretization is governed by the complexity of the geology, i.e., fractures, faults, pinchouts, lateral, and vertical heterogeneity, etc. Therefore, different gridding schemes were used, such as structured and unstructured gridding.

Structured grids are three-dimensional (3D) Cartesian grids, which can be defined using the number of cells in each dimension (x, y, and z directions). Accordingly, structured grids inherit the ease of cell indexing from its Cartesian nature. For example, a triplet of three integers (i, j, and k) can reference cells. Furthermore, a region can also be defined using two triplets of the form $(i_{\text{start}}, j_{\text{start}}, k_{\text{start}})$ and $(i_{\text{end}}, j_{\text{end}}, k_{\text{end}})$. The region in this case is nothing but a rectangular cuboid; however, structured grids have a few caveats when it comes to modeling complex reservoir features such as fractures, faults, and near wellbore regions. This is due to cells being limited in their shapes, i.e., Cartesian nature of the grid. They cannot take more complicated and detailed shapes to represent and preserve complex geological features. For these reasons, unstructured grids were introduced, and found to be more suitable.

Unstructured grids are grids where cells are allowed to take any polyhedral shape. This gridding scheme allows the modeling of complex geological features and near wellbore modeling. Compared to structured gridding, unstructured gridding offers computational efficiency and accuracy when local grid refinement/coarsening is used. One of the flavors of unstructured gridding schemes is the 2.5D unstructured gridding approach. It is a special case, where the grid is divided into identical layers in terms of geometry and number of layers.

The cells within a layer take prism-like shapes, having tops and bottoms that can be of any polygon shape. Subsequently, we will be referring to them simply as “unstructured grids.” The 2.5D unstructured grids provide a compromise between structured and fully unstructured grids, having the freedom in the geometrical shapes in lateral directions, with retention of structure in the vertical direction.

These features overcome the aforementioned limitations of structured grids and avoid the unnecessary complexity of the fully unstructured gridding scheme; however, with the flexibility of cell shapes comes different challenges. In particular, unstructured grids lose the ease of indexing in the x and y directions, and cells within a layer can only be indexed using an irregular numbering scheme. Instead, each cell has a unique ID that may not necessarily be in sequence or following a certain order. In addition, these IDs do not encode any spatial reference of the whereabouts of the cells within the grid. Consequently, to specify a single region in an unstructured grid, one must list contiguous cell IDs, which is an arduous task to do manually.

In this article, we leverage algorithms from computational geometry to alleviate the cell’s indexing problem in unstructured grids by:

- Efficiently converting regions from the structured domain to the unstructured domain.
- Providing the ability to select arbitrary prism-like regions in unstructured grids.
- Developing a graphical interface to interactively make region selections.

The algorithm could also be used with the structured format to select arbitrary regions rather than only cuboid ones. As the basis for the proposed solution, 2D range trees were used. These 2D range trees are data structures to hold d-dimensional Euclidean points, where the points are dictionary sorted by their coordinates. They are used to answer orthogonal range reporting queries; that is, each query is the Cartesian product of intervals of real numbers. They were developed independently by a handful of authors²⁻⁵.

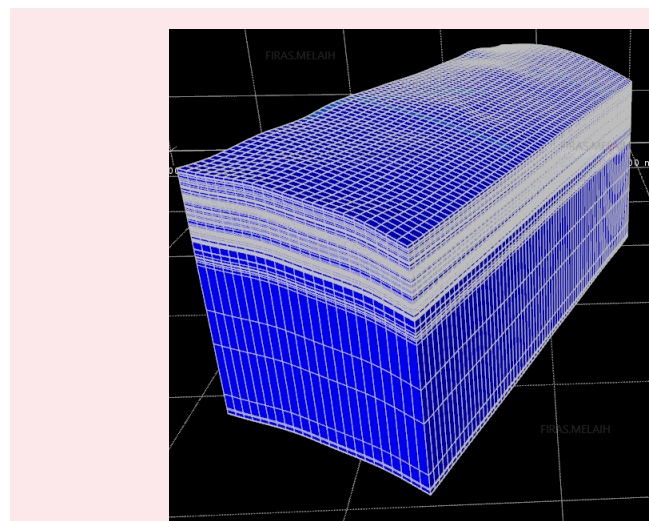
This article will describe how the algorithms are used, as well as describe how to implement fractional cascading^{4,6} to improve their query time complexity, while not increasing the space complexities, nor the preprocessing time complexity.

Problem Definition

Let us start by properly defining the problem: A 2.5D unstructured grid is given — where the 2.5D grid means all the layers are identical in the x and y directions — and a prism-like region, R , specified with a triplet of (x, y, and z) coordinates. The top and bottom sides of R are the same polygon, P , and the height of the top and bottom is specified by the layer number, Fig. 1. The goal is to find the IDs of all the cells of the grid that intersect R .

Usually, the grid will be queried many times with different regions. From the computational efficiency viewpoint, the algorithm efficiency heavily depends on the reservoir model size — number of cells — and the irregularity of the selected regions. In simple cases, a handful of queries will not take more than a few seconds when it is solved,

Fig. 1 A region of a 2.5D unstructured grid.



by simply checking R against every cell. This problem becomes time-consuming, less efficient, and computationally expensive with the increasing complexity of the region and model's number of cells. A viable solution was devised and is described later.

Simplification

The first step toward computational efficiency is simplifying the problem to a 2D problem. R is simply considered a prism. Therefore, its layers can be specified in the usual way, and we can focus on the problem in the lateral directions. Subsequently, we effectively reduced this problem from a 3D problem to a 2D problem.

We can further simplify the problem by observing that a cell intersects P if one of its corners is inside P , Fig. 2. This turns it into the simpler problem of finding the points that lie inside P . This type of problem is called polygonal range searching. Therefore, n will denote the number of points in a single layer of our grid.

There are exceptions to this simplification such as edge cases, Fig. 3. These cases occur when a cell does not have any corners inside P , but the edges of both the cell and P intersect, e.g., if a corner of P is inside the cell. This can be remedied by checking nearby neighbors if they intersect P , and then adding them to the solution if

they do. We can precompute which cells in a layer are neighboring each other to save time.

Approaches

Solving the problem in the naïve way, where every point is checked whether it lies in P or not, is efficient memory-wise, as it uses no memory overhead, and also is efficient time-wise if a query is made once, or only a handful of times. The complexity of the query time of this solution is $O(n)$, while the space complexity is $O(k)$ for a query (and $O(n)$ for storing the points), where k is the number of points inside P . (This is in fact the optimal solution, and we cannot do any better.) Consequently, if the model size is large, say 5 million points per layer, and with 200 regions to query, then 1 billion checks are required, going over all the points.

This is why there is a need for preprocessing the points to satisfy all these queries. There is no algorithm tailored for polygonal range searching, specifically in the literature. It can be reduced to other problems via triangulation or other means. We opted to reduce the problem in a different way: To find the bounding box (B) of P , apply a 2D orthogonal range searching algorithm, and then filter the results with the winding number algorithm. Figure 4 shows an example of a P and its B .

For efficiency, the winding number algorithm should be embedded within the orthogonal range searching during appending to the results list. This is to decrease the amount of extra memory to be used. It is counterproductive to include the points inside B but outside P .

There are two main approaches to solving the orthogonal range searching: k-d trees and 2D range trees. We will be using the 2D range tree algorithm in this article. The 2D range trees have a preprocessing time cost of $O(n \log(n))$, which we only have to do once, and a query time complexity of $O(\log(n) + k)$, which is extremely fast in comparison to the $O(n)$ of the naïve method.

Fig. 2 A sample image showing that a cell intersects P if one of its corners is inside P .

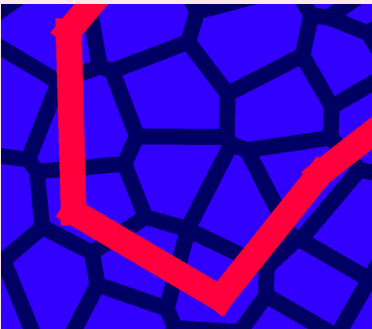


Fig. 3 None of the corners of the bottom left cell are inside, yet it still intersects.

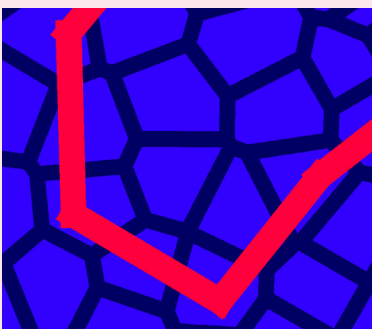
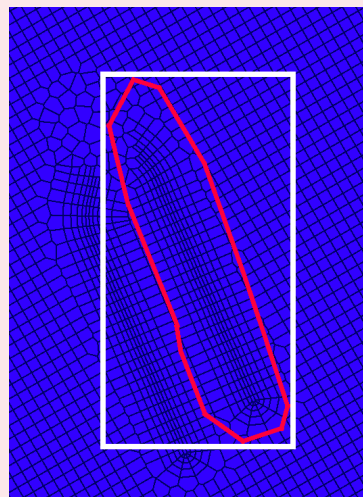


Fig. 4 The P shown in red, with its B in white.



The trade-off is in the space cost, where the naïve method has a space complexity of $O(n)$, while the 2D range tree has a space complexity of $O(n \log(n))$. This is a point that needs to be emphasized: The tree must be saved as a file after construction, to be used again for later queries. Otherwise, it would have to be constructed every time there is a need to query a set of regions.

2D Range Tree

The idea of a 2D range tree, T , is to have a binary tree ordered by the x coordinates of the points, and then each node, N of T , contains a binary tree called the associated tree $A(N)$, Fig. 5. It consists of only the points in N 's subtree, and it is ordered by the y coordinate. This is the reason the space complexity of T is $O(n \log(n))$; every one of the $O(\log(n))$ levels contains a duplicate of the original n points, where the points are divided among the nodes of the level in the associated trees.

The query is computed by traversing T until reaching the split node, S , a node where there are points with x coordinates between the x coordinates of B in both branches of S . Once there, two traversals occur, one to the left branch, and one to the right branch. Each traversal goes to its respective leaf with the x coordinate of B — or the closest coordinate inside B — while collecting points within P on the way there. Fractional cascading is also used in the algorithm to ensure that the time complexity of the query is $O(\log(n)+k)$ rather than $O(\log(n)^2+k)$.

Range Tree Preprocessing

The first step of preprocessing is to make a copy of the

layer's points and replace the coordinates with ranks. Ranks are the indices of the points when they are dictionary sorted, i.e., the x rank of a point, p , denoted as $r_x(p)$, is the index of p when the points are dictionary sorted by x first and y second, and the y rank, $r_y(p)$, is the index of p when the points are dictionary sorted by y first and x second. The replacement is to remove (x, y) and use $(r_x(p), r_y(p))$ instead. The reason ranks are used instead of the coordinates directly is that ranks ensure that each pair of numbers is distinct in both entries.

Then, the rank pairs are dictionary sorted by the y ranks, and passed to the root of the tree. This is the beginning of the recursive construction process: At each node, N , N will be passed at the $A(N)$, which it will keep, as well as assigning itself the x rank in the middle of $A(N)$. Then, it will make a copy of $A(N)$ to be split into two halves based on whether the x rank is higher or lower than the N 's x rank. Next, these two halves will be passed to the respective child nodes. N_L and N_R will denote the left and right children, respectively.

After the children are done, the cascading will be added to N . In this step, for each of the two child nodes, an array will be created with the same size as $A(N)$, denoted by $C_L(N)$ and $C_R(N)$ for the left and right children, respectively. $C_L(N)[i]$ will store an index j , where $A(N)[i] \leq A(N_L)[j]$, but $A(N)[i] > A(N_L)[j-1]$. In other words, $C_L(N)[i]$ will point to the earliest entry in $A(N_L)$, which is greater than $A(N)[i]$, and similarly for the right side. If no such j exists, then it will store the size of $A(N_L)$. Figure 6 shows the cascading.

Fig. 5 A 2D range tree, where each node has an associated tree?

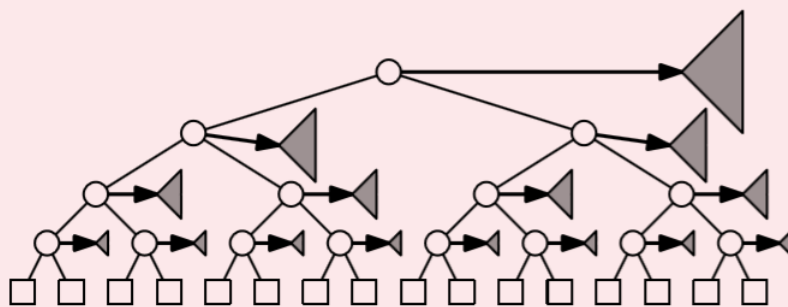
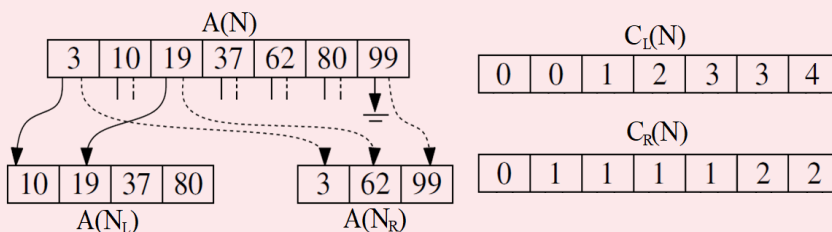


Fig. 6 Example of fractional cascading (some omitted)?.



For example, in Fig. 6, $A(N)[2] = 19$ (using 0-based indexing), and the earliest entry in $A(N_R)$ that is greater than or equal to 19 is 62 at index 1. Therefore, in $C_R(N)[2]$, the value is 1, which is the index of 62 in $A(N_R)$. For $A(N)[6] = 99$, there is no entry in $A(N_L)$ that is greater than or equal to 99, and so it simply contains 4, which is the length of $A(N_L)$, so that it acts as a sentry.

Without fractional cascading, at each stage of the query, a binary search must be done to find the smallest y rank in $A(N)$ that is inside B , and all these binary searches will add up to an $O(\log(n)^2)$ time complexity. Instead, we can eliminate them almost entirely with fractional cascading, having only to do one binary search at the S , and then traversing the fractional cascades, as they will land on the first such y rank inside B .

Range Tree Query Algorithm

For the query, the first step is to find the B of P via the minimum and maximum of the x and y coordinates of the vertices of P . Then, B 's x coordinates are translated into ranks by binary searching for the minimum and maximum ranks of points that lie within B 's x coordinates. Using these two extreme ranks, we traverse T to find the S —this is achieved by choosing the child nodes that contain both ranks at every level until they are not contained in the same child.

Once S is found, two binary searches are done to find the extreme y ranks, similar to the step done earlier for x . This is done now and not with x because it is more efficient to search the smaller array, $A(S)$, rather than the large A of the root. Two traversals are done at this part of the algorithm: One to the left branch, and one to the right branch, both going down to the leaves to reach the extreme x ranks.

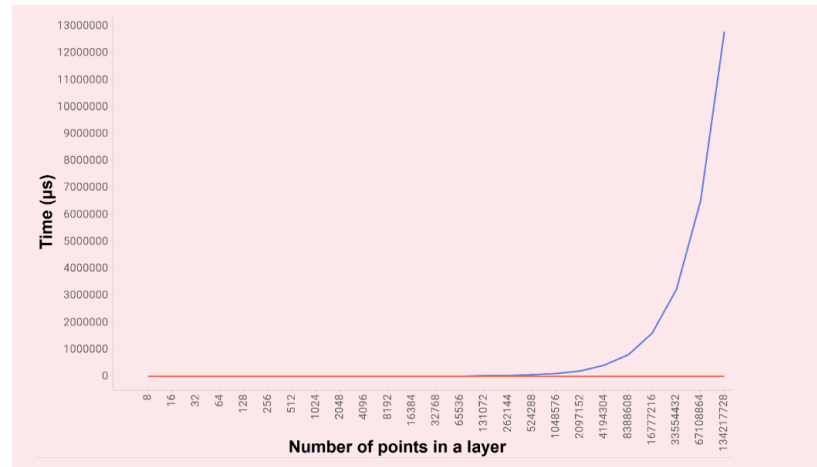
In the sequel, the “outer node” will refer to the node in the same direction of the traversal, and the “inner node” will refer to the node opposite the direction of the traversal, i.e., if traversing the left branch, the left children are the outer nodes, and the right children are inner nodes, and the opposite holds for the right branch. Whenever the inner node is taken, nothing is to be done, and the traversal continues. Whenever the outer node is taken, all the rank pairs in the inner nodes will have x ranks contained in the x bounds of B .

These pairs will be checked against the query P for containment using the winding number algorithm. Following the cascade, pointers will guarantee that the checking starts at the earliest pair with a y rank contained in B , and the checking can stop once the y rank lies outside B .

Results

In Fig. 7, we compare the naïve linear approach against the range tree approach. The x -axis denotes the number of points tested (where it is for a single layer), and the y -axis denotes the amount of time taken in microseconds. Along the x -axis, the number of points starts from eight, and doubles with every iteration. The query is simply a 10×10 square near the center of the layer. The reason behind choosing a small region is the time complexity (cost) of the range tree query, which is $O(\log(n)+k)$. This means that having a larger region will result in the k

Fig. 7 The input size (number of layer points) plotted against the amount of time taken by each algorithm in microseconds; naïve in blue, range tree in red.



dominating the term, and therefore, both algorithms will have similar times, and the difference will not be noticeable.

As the number of points grow, the amount of time taken by the naïve algorithm is proportional to it. This is clear as seen in the log-scale graph in Fig. 8, where a line almost perfectly fits on the log base 2 of the input size and the log base 2 of the algorithm time.

On the other hand, the range tree approach only takes a logarithmic amount of time. Given a layer with 134 million points (2^{27}), the query time for the naïve algorithm was 12.7 seconds. Therefore, if we were to suppose that we needed to do this for 1,000 regions, this would take over 3.5 hours. Conversely, the range tree algorithm took only 232 microseconds, and 1,000 queries would take it 0.23 seconds. Table 1 lists the input size vs. time taken in microseconds.

Figure 9 shows a graphical interface, which was implemented to simplify the region's selection. This allows for inspecting, adding/deleting, and editing the regions.

Fig. 8 The naïve algorithm takes a linear amount of time.

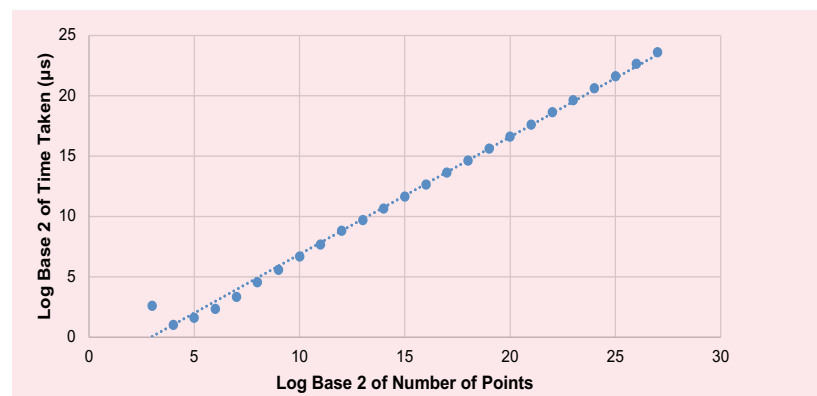


Table 1 Input size vs. time taken in microseconds by both algorithms.

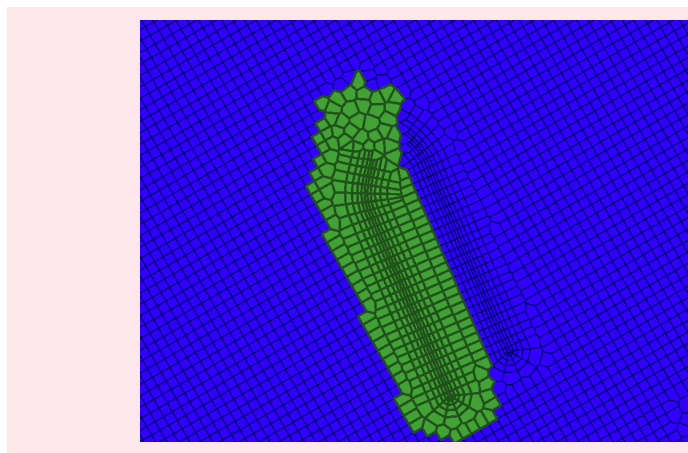
Number of Points	Naïve Time (μ s)	Range Tree Time (μ s)
8	6	19
16	2	4
32	3	8
64	5	9
128	10	13
256	23	18
512	48	19
1,024	101	20
2,048	201	21
4,096	442	21
8,192	827	22
16,384	1,588	23
32,768	3,180	34
65,536	6,297	57
131,072	12,558	76
262,144	25,279	133
524,288	50,505	301
1,048,576	100,392	95
2,097,152	200,640	150
4,194,304	402,064	146
8,388,608	801,379	140
16,777,216	1,602,892	137
33,554,432	3,216,354	143
67,108,864	6,520,000	264
134,217,728	1,278,7232	232

It also facilitates the translation between what is envisioned by the engineers to the simulation model input data and vice versa.

Conclusions

To address mapping between structured and unstructured (2.5D) domains, an efficient workflow was developed to automatically transform the modeling of property modifiers for near wellbore modeling and local grid refinement/coarsening between the structured and unstructured domains. Several computational geometry algorithms were developed and assessed for efficiency and accuracy. The regions are then translated into an unstructured

Fig. 9 An image of the graphical interface to the range tree algorithm.



format of the targeted reservoir simulator.

It has been shown that range trees are a viable option to efficiently select regions in grids, whether structured or unstructured, as long as there is a large number of such regions that needs to be created and/or converted. The difference between the range tree approach and the naïve approach in terms of time is huge; the range tree approach takes only fractions of a second to accomplish what the naïve approach can do in hours. This is in agreement with the theory. Its trade-off in the memory footprint is justifiable if there is a large number of regions, where the strength and computational efficiency is demonstrated.

Acknowledgments

This article was prepared for presentation at the European Association of Geoscientists and Engineers Conference and Exhibition, Amsterdam, the Netherlands, December 8-11, 2020.

References

1. Dogru, A.H., Fung, L.S.K., Al-Shaalan, T.M. and Pita, J.A.: "From Mega Cell to Giga Cell Reservoir Simulation," SPE paper 116675, presented at the SPE Annual Technical Conference and Exhibition, Denver, Colorado, September 21-24, 2008.
2. Bentley, J.L.: "Decomposable Searching Problems," *Information Processing Letters*, Vol. 8, Issue 5, June 1979, pp. 244-251.
3. Lee, D.T. and Wong, C.K.: "Quintary Trees: A File Structure for Multidimensional Database Systems," *ACM Transactions on Database Systems*, Vol. 5, Issue 3, September 1980, pp. 339-353.
4. Lueker, G.S.: "A Data Structure for Orthogonal Range Queries," paper presented at the 19th Annual Symposium on Foundations of Computer Science, Ann Arbor, Michigan, October 16-18, 1978.
5. Willard, D.E.: "The Super-B-Tree Algorithm," Technical Report, Harvard University, Cambridge, MA: Aiken Computer Lab, 1979, 39 p.
6. Willard, D.E.: *Predicate-Oriented Database Search Algorithms*, New York: Garland Publication Company, 1979, 384 p.

7. van Kreveld, M.: "Lecture 8: Range Trees," presentation, 61 p. <http://www.cs.uu.nl/docs/vakken/ga/2019/slides/slides5b.pdf>.
8. de Berg, M., Cheong, O., van Kreveld, M. and Overmars, M.: *Computational Geometry: Algorithms and Applications*, 2nd edition, Springer-Verlag, 2008, 379 p.

About the Authors

Firas H. Melaih

*B.S. in Computer Science,
King Fahd University of Petroleum
and Minerals*

Firas H. Melaih is a Petroleum Engineering Systems Analyst working in the Simulation Systems Division of Saudi Aramco's Petroleum Engineering Application Services Department. His primary interests include algorithms and mathematics.

In 2018, Firas received his B.S. degree in Computer Science from King Fahd University of Petroleum and Minerals (KFUPM), Dhahran, Saudi Arabia.

Dr. Ali A. Al-Turki

*Ph.D. in Petroleum Engineering,
University of Calgary*

Dr. Ali A. Al-Turki is a Petroleum Engineering Systems Specialist working in the Simulation Systems Division of Saudi Aramco's Petroleum Engineering Applications Services Department. Ali has been with Saudi Aramco for the past 21 years.

His research interests include multiphase flow in fractures, thermal (SAGD) and thermal solvent (ES-SAGD) recovery processes, assisted history matching methodologies, uncertainty quantification and management, and high performance computing.

Ali is a Society of Petroleum Engineers (SPE) Certified Petroleum Engineer.

He is the author and coauthor many technical papers, along with a number of patents.

Ali received his B.S. degree in Computer Science from King Fahd University of Petroleum and Minerals (KFUPM) Dhahran, Saudi Arabia. He received both his M.S. and Ph.D. degrees in Petroleum Engineering from the University of Calgary, Alberta, Canada.

Dr. Razen M. Al-Harbi

*Ph.D. in Computer Science,
King Abdullah University of Science
and Technology*

Dr. Razen M. Al-Harbi is a Petroleum Engineering System Analyst working in the Simulation Systems Division of Saudi Aramco's Petroleum Engineering Applications Services Department. Razen is leading the Fourth Industrial Revolution team in his Division to enable artificial intelligence and machine learning technologies in simulation systems.

His primary research interest includes optimizing massively parallel applications running on large installations of high performance computing (HPC)

systems and data analytics on HPC infrastructure.

Razen received his B.S. degree in Information and Computer Science from King Fahd University of Petroleum and Minerals (KFUPM), Dhahran, Saudi Arabia, in 2006. Then, he received his M.Eng. degree in 2006 from Cornell University, and his Ph.D. degree in Computer Science from King Abdullah University of Science and Technology in 2016.

Dr. Majdi A. Baddourah

*Ph.D. in Civil Engineering,
Old Dominion University*

Dr. Majdi A. Baddourah is a Simulation and High Performance Computing Specialist working in the Simulation Systems Division of Saudi Aramco's Petroleum Engineering Application Services Department.

Prior to joining Saudi Aramco in 2003, Majdi worked for Lawrence Berkeley National Laboratory, CA conducting research and development for the U.S. Department of Energy, utilizing high performance computers. He also worked at the NASA Langley Research Center, VA as a High Performance Specialist. Majdi is a key supporter for POWERS and GigaPOWERS, providing support for Saudi Aramco's strategic studies.

He also works with the EXPEC Computing

Planning and Technology Division and the EXPEC Computer Operations Department as an active technologist in evaluating the deployment of state-of-the-art high performance computing solutions at minimal cost.

Majdi is the author and coauthor of numerous technical papers. He also holds many U.S. patents. Throughout Majdi's extensive career, he has mentored many young professionals.

Majdi received both his B.S. degree and M.S. degree in Civil Engineering from the University of South Carolina, Columbia, SC. He received his Ph.D. degree in Civil Engineering from Old Dominion University, Norfolk, VA.

A Novel Polymer to Create a New Approach of Hole Cleaning

Meshari M. Alshalan, Dr. Abeer M. Al-Olayan, Mohammed M. Al-Rubaii, and Timothy E. Moellendick

Abstract /

A new type of drilling fluid, based on a crosslinker, was developed using polymer chemistry to create a superior hole cleaning product that moves drill cuttings, metal, shavings, and other debris out of the wellbore. In addition, the new polymer is capable of transporting cuttings when drilling metallic junk or partial loss of the formation. The gel is generated by adding a crosslinker (borax) to the drilling fluid, and then spotting the second component (polyvinyl alcohol (PVA)) diluted with water at designed percentages. The gel is spotted in the wellbore and then washed out.

The strong carrying capacity of the gel is expected to remove all cuttings and debris from the wellbore. The other conventional hole cleaning pills contain large solids and/or are expensive. The other method to clean excessive junk from the wellbore is mechanically, by running many hole cleaning trips, which consumes a lot of rig time.

This practice has saved time by reducing the clean out trips. Moreover, the new product, coined “polysweep” can provide a potential solution to hole cleaning when milling metallic junk or drilling at partial circulation. Polysweep has been successfully trial tested in a deviated well — with partial losses. During the field trial, it was observed that polysweep was effective in carrying all the shaving debris and cuttings out from the wellbore throughout the drilling operation with no trouble. Also, polysweep has shown good compatibility for use in water-based drilling fluids.

Polysweep brings value through both its cost-effective, simple formulation, as well as its ability to reduce the number of wiper trips. Besides that, it is environmentally friendly as all the components of the fluid are nontoxic. The new composition has the potential of producing modified fluids for several different applications, including hole cleaning sweeps, loss circulating materials, and fracturing fluids.

Introduction

Optimization of hole cleaning during a drilling operation is very important to enhance the drilling rate, however, optimum hole cleaning in drilled hole sections remains a major challenge. Hole cleaning must be engineered. The penetration rate is highly dependent on hole cleaning. Insufficient hole cleaning can cause numerous issues, including stuck pipes, decreased drilling rates, significant drag and torque, lost circulation, wellbore instability, erratic trends in equivalent circulating density, more wiper trips, back reaming, bad quality of cement jobs, bit balling, and obviously increases in the cumulative cost of drilling operations and the extension of the overall operational time¹.

If inadequate attention is paid to hole cleaning, such problems can be a root cause of losing the well. To overcome these problems, drilled cuttings should be efficiently transferred from the hole section by drilling fluid to the surface. Hole cleaning is a key element of all successful well design strategies and the issue cannot be over emphasized in horizontal or maximum reservoir contact wells in particular².

Hole cleaning is often the deciding factor between the success and failure during drilling. Historically, most stuck pipe incidents can be attributed to poor hole cleaning³. It is very important to identify any wellbore stability problems that are affecting the hole cleaning before making changes to the initial planned hole cleaning strategy. Hole cleaning is more difficult with oil-based mud (OBM) due to the following reasons: (1) the cuttings will not easily disperse into the OBM as with water-based mud (WBM), (2) OBM is more Newtonian than WBM, and (3) OBM has lower thixotropic properties than WBM⁴.

To achieve optimum hole cleaning it is necessary to increase the flow rate to achieve annular velocity to more than the slip velocity, while simultaneously optimizing mud rheology to increase the transport ratio. Theoretically, if the annular velocity is more than the slip velocity, the mud will lift the drilling cuttings and ultimately the drilling cuttings will be transported out of the wellbore. A low annular velocity can cause an unwanted volume of cuttings in the annulus. Several drilling case studies have proven that if the cutting's concentration or cutting's volume in the annulus is more than 5%⁵, it can lead to a tight hole, stuck pipe, or induced loss circulation events.

Inadequate hole cleaning can make drilling cuttings accumulate in the annulus of the open hole section, and as a result, cause the drilling rate to decrease. Drilling in complicated geological zones, such as faults, joints,

fractures, layered formations, weak bedding planes, etc., normally cause instability problems for the hole section, therefore, a better understanding of the geomechanics of the fracturing of the formation will act as an important solution to cure the problems of hole sections⁶. The instability problems of the hole section can be caused by the effect of mechanical influences, chemical influences, or a combination of them.

The density of the mud — too high or too low — as well as the drilling mud parameters and bad operational practices often causes mechanical wellbore damage. This damage may include excessive vibration, high torque and drag, and not performing wiper trips if the hole section dictates⁷. On the other hand, chemical wellbore damage is caused by use of improper drilling fluids or improper concentrations of inhibitors added while drilling reactive shale formations⁸. If the hole starts to have sloughing or caving problems, the quantity of shale transferred to shakers may appear normal, masking the large quantity that may accumulate in the annulus.

Hole cleaning is a common problem encountered while drilling. The consequences of inadequate hole cleaning vary depending on several factors, such as the rate of penetration, the loss severity, and the criticality of the drilled zone⁹. Several materials and methods for optimizing hole cleaning are used globally. Consequently, most of them have shown weakness dealing with the breadth of the required applications, particularly in deviated sections. The main object of any hole cleaning optimization product is to enhance the ability of the mud system to carry out the cuttings all the way to the surface, effectively and economically¹⁰. Polysweep is a combination of two fluids that will generate a gel phase in seconds after mixing. The created gel is strong enough to remove the drilling cuttings to the surface, even in the most difficult operational environments.

In addition, the same cross-linked synthetic technology (polysweep) can also provide a potential solution to mud losses in high permeable and fractured loss zones. The components used in the formulation react quickly to form a gel with flexible and ductile characteristics, and therefore can provide an effective solution for stopping lost circulation in fractures and high permeable zones. Due to flexible, ductile and deformable characteristics, it can easily mold into the fractures and high permeable zones to produce superior sealing and blocking.

The reaction to form the gel is very fast and does not require special conditions to trigger the reaction. Due to very quick reaction time, the components have to be placed in the loss zone separately to create the gel in situ. One of the components can be added to bentonite mud, and the other component can be pumped to introduce it into the bentonite mud in the vicinity of the loss zone to convert the combined products into a stiff gel. All lab tests were conducted successfully prior to the request of a field trial.

Laboratory Development and Assessment

Compressive Strength

In this test, the compressive strength of the final polysweep

material was tested using a stable micro-system, Fig. 1. The test was conducted with different ratios of the crosslinker (borax) and polyvinyl alcohol (PVA) to reach to the optimum ratio that makes the polymer rigid, and at the same time pourable and flexible to allow it to move through the pores. The results show that the strength of the polymer was increased with the increase of the borax concentration ratio, Figs. 2a, 2b, and 2c.

Sealing and Blocking Efficiency Evaluation

Simulating High Permeable loss zone (CaCO₃ bed). To evaluate the sealing and blocking efficiency of the polysweep, we used a low-pressure, low temperature (LPLT) test apparatus designed by a Saudi Aramco scientist and high permeable carbonate bed material to simulate a high permeable loss zone, Fig. 3. The LPLT cylinder has a diameter of 7.5 cm and a length of 26.5 cm. The carbonate bed has a measured porosity of 50%.

In this test, the sealing efficiency of the polymer was evaluated by simulating a very high permeable bed made of 4 mm to 6 mm sized carbonate particles. To measure the blocking and sealing efficiency of the polysweep, we conducted tests using drilling mud to simulate a loss circulation event, and then we mixed one component of the polysweep with the drilling fluid, and let it soak

Fig. 1 An image showing the stable micro-system model.

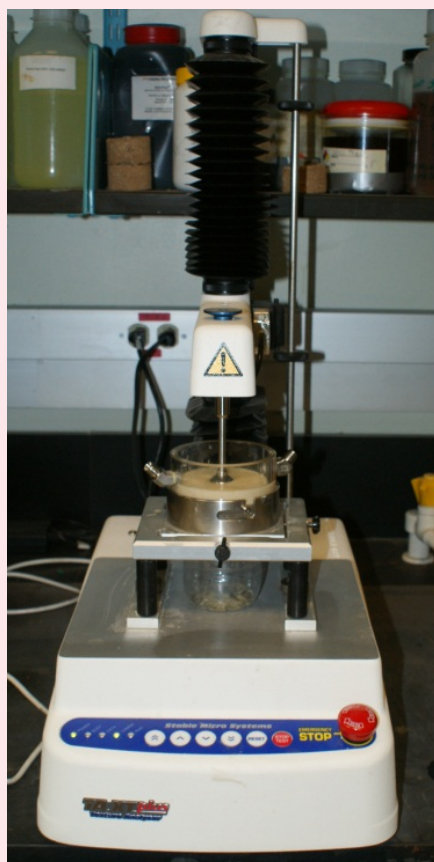


Fig. 2 The strength of the polymer was increased with the increase of the borax concentration ratio.

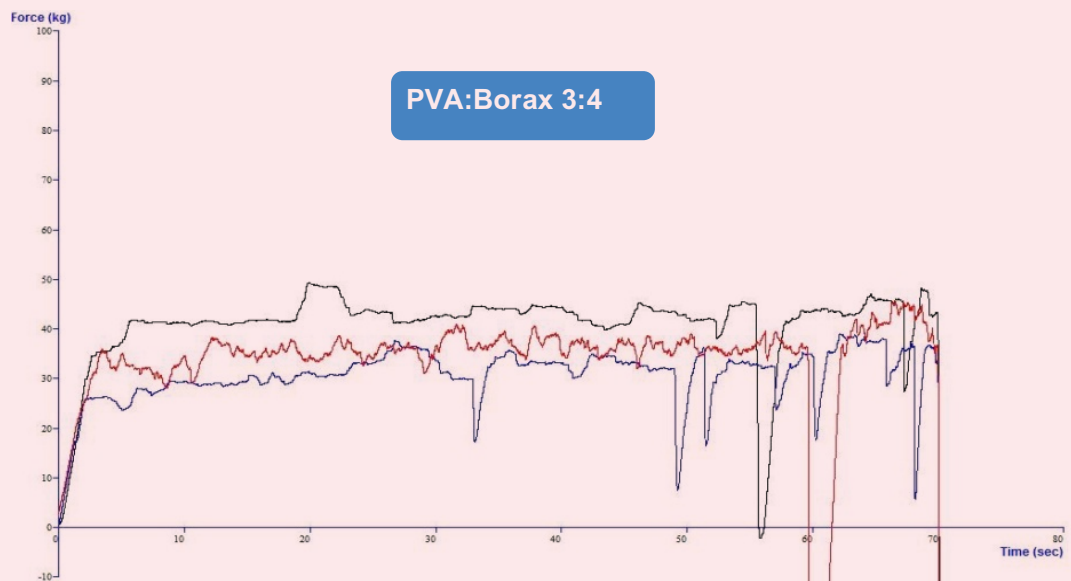
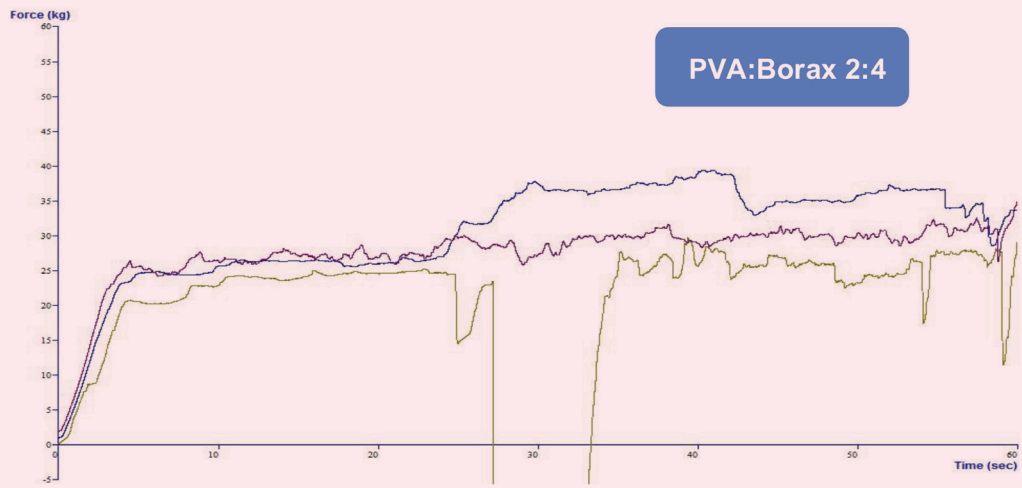
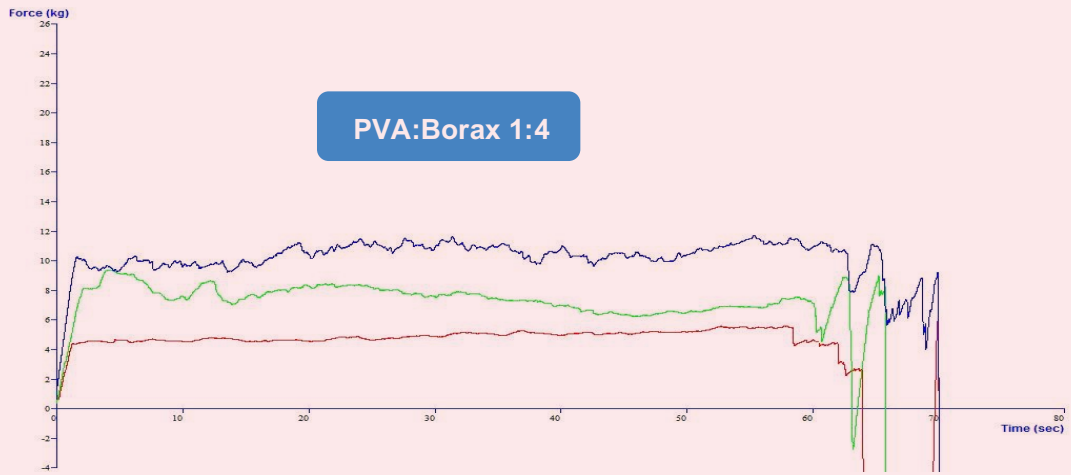
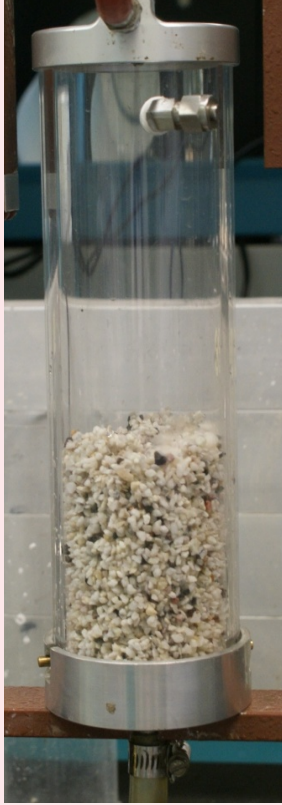


Fig. 3 The LPLT test apparatus filled with high permeable carbonate bed material.



for 10 minutes. After that, the other component of the polysweep was added to the mud to measure the sealing and blocking efficiency of the polysweep. We applied a pressure of 100 psi to simulate the overbalance pressure of the borehole at room temperature.

The polysweep was tested and compared to two commercial products used by Saudi Aramco: Stoploss and Soluseal. All tests were conducted three times.

The result shows that both polysweep, Fig. 4a, and Soluseal, Fig. 4b, have a high capacity to plug the pores and prevent the drilling fluid to pass through. On the contrary, stoploss, Fig. 4c, has no ability to plug the pores, and all the liquid passed through.

Simulating Super-K loss zone (Pebble bed).

To evaluate the sealing and blocking efficiency of the polysweep for a super permeable zone, the pebble bed was used to simulate it, Fig. 5a. The result shows that polysweep alone could not plug the pores and all the fluid passed through, Fig. 5b. The test was run again, but this time polysweep was added. The process was conducted in two steps: (1) polysweep was added first and left to soak for 10 minutes, and (2) then date tree roach root fibers was added. This time, the sealing was excellent, plugging the pores completely, not allowing any fluids to pass through, Fig. 5c.

Thermal Stability

The polymer was tested for different temperatures and pressures to evaluate its stability under well conditions. Figure 6a shows the test sample conducted at 80 °F with no pressure. Figure 6b shows the test sample conducted at 150 °F and 500 psi, using static pressure. Figure 6c

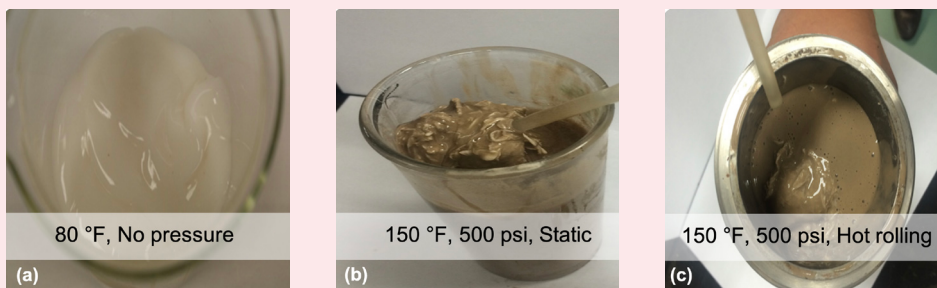
Fig. 4 The LPLT test conducted using carbonate bed material for (a) polysweep, (b) Soluseal, and (c) stoploss.



Fig. 5 The LPLT test using pebble bed for (a) polysweep, (b) polysweep system, and (c) polysweep plus date tree roach root fibers.



Fig. 6 Images of the polymer after testing to evaluate its stability under well conditions: (a) at 80 °F with no pressure, (b) at 150 °F and 500 psi, using static pressure, and (c) at 150 °F and 500 psi, after hot rolling.



shows the test sample conducted at 150 °F and 500 psi, after hot rolling.

These tests were to observe the attitude of the polymer when increasing the temperature and pressure. The results showed that the polymer is formed direct and the solidification is increased with temperature and pressure. Importantly, the polymer does not show any degradation at these conditions.

Field Trial Test

The developer completed trial tests for polysweep observing the results, and conducted comprehensive lab tests that showed promising results in regard to hole cleaning efficiency. The polysweep is produced when two fluids, one containing PVA and one containing borax, react together. The generated mixture is a strong

polymer gel that can remove the cuttings and seal any loss circulation zones.

The field trial was conducted recently. The well encountered partial losses during drilling the 16" hole section at 1,594 ft. The rig laid down the drilling assembly and ran open-ended drillpipe to the top of the loss zone. The rig spotted 140 bbl of the polysweep (15 bbl of hi-vis spacer, 90 bbl of polysweep, 15 bbl hi-vis spacer, and 20 bbl caustic pill) across the loss zone. Static losses dropped to zero. The rig laid down open-ended drillpipe, ran the drilling assembly to the bottom, and resumed drilling with 100% circulation, and all the cuttings that were in the hole were transported to the surface successfully.

Conclusions

The developed crosslinker (polysweep) is a superior hole cleaning product that transports drill cuttings, metal shavings, and other debris out of the wellbore.

- Two fluids when mixed downhole generate gel that has a high carrying capacity.
- The polymer is compatible for use in water-based drilling fluids.
- The gel lifts and carries metal shaving debris during milling operations and provides a reliable solution in partial circulation conditions.
- The polymer helps minimize the number of wiper trips.
- The gel is nontoxic and chemically inert.

Acknowledgments

This article was previously presented at the International Petroleum Technology Conference, Dhahran, Saudi Arabia, February 13-15, 2020.

References

1. Al Rubaii, M.M.: "A New Robust Approach for Hole Cleaning to Improve Rate of Penetration," SPE paper 192223, presented at the SPE Kingdom of Saudi Arabia Annual Technical Symposium and Exhibition, Dammam, Saudi Arabia, April 23-26, 2018.
2. Al Rubaii, M.M., Sehsah, O.R. and Omini, E.: "Approach to Improve Well Drilling Performance," SPE paper 194223, presented at the SPE Kingdom of Saudi Arabia Annual Technical Symposium and Exhibition, Dammam, Saudi Arabia, April 23-26, 2018.
3. Pigott, R.J.S.: "Mud Flow in Drilling," API paper 14-091, presented at the Drilling and Production Practice Conference, New York, New York, 1941.
4. Hossain, M.E. and Al-Majed, A.A.: *Fundamentals of Sustainable Drilling Engineering*, Wiley, March 2015, 786 p.
5. Moore, P.L.: "Five Factors That Affect Drilling Rate," *Oil and Gas Journal*, Vol. 56, No. 40, 1968, pp. 141-170.
6. Al Rubaii, M.M., Al Yami, A.S. and Omini, E.: "A Robust Correlation Improves Well Drilling Performance," SPE paper 195062, presented at the SPE Middle East Oil and Gas Show and Conference, Manama, Kingdom of Bahrain, March 18-21, 2019.
7. Nwagu, C., Awobadejo, T. and Gaskin, K.: "Application of Mechanical Cleaning Device: Hole Cleaning Tubulars, to Improve Hole Cleaning," SPE paper 172403, presented at the SPE Nigeria Annual International Conference and Exhibition, Lagos, Nigeria, August 5-7, 2014.
8. Caenn, R., Darley, H.C.H. and Gray, G.R.: *Composition and Properties of Drilling and Completion Fluids*, 7th edition, Elsevier Inc., 2017, 748 p.
9. Adari, R.B., Miska, S., Kuru, E., Bern, P., et al.: "Selecting Drilling Fluid Properties and Flow Rates for Effective Hole Cleaning in High-Angle and Horizontal Wells," SPE paper 63050, presented at the SPE Annual Technical Conference and Exhibition, Dallas, Texas, October 1-4, 2000.
10. Larsen, T.I., Pilehvari, A.A. and Azar, J.J.: "Development of a New Cuttings Transport Model for High-Angle Wellbores including Horizontal Wells," *SPE Drilling & Completion*, Vol. 12, Issue 2, June 1997, pp. 129-136.

About the Authors

Meshari M. Alshalan

*B.S. in Petroleum Engineering,
University of Leeds*

Meshari M. Alshalan is a Petroleum Engineer working with the Drilling Technology Team of Saudi Aramco's Exploration and Petroleum Engineering Center – Advanced Research Center (EXPEC ARC). Meshari works on number of projects that are focused on advanced drilling and workover methods, as well as developing cost-effective

methods for reducing drilling expenses.

In 2016, he received his B.S. degree in Petroleum Engineering from the University of Leeds, Leeds, U.K. Meshari is currently pursuing an M.S. degree in Petroleum Engineering as a part-time student at King Fahd University of Petroleum and Minerals (KFUPM), Dhahran, Saudi Arabia.

Dr. Abeer M. Al-Olayan

*Ph.D. in Analytical Chemistry,
King Faisal University*

Dr. Abeer M. Al-Olayan is a Senior Research Scientist and the Head of Upstream Commercialization at Saudi Aramco's Exploration and Petroleum Engineering Center – Advanced Research Center (EXPEC ARC). Abeer is also Project Leader at the Saudi Aramco Global Research Centers in the U.S. and at MIT.

She was an Assistant Professor with the Chemistry Department of Dammam University before joining Saudi Aramco in 2011.

Abeer has an academic and industrial background with more than 19 years of experience in chemistry and related applications.

She is the recipient of the Woman of the Year Award for Oil and Gas and Petrochemicals in the Middle East for 2017-2018, as well as other local, regional, and international awards. Abeer was selected as one of the top 100 elite figures in

Global Energy by the British *Petroleum Economist* magazine.

She is a Visiting Scientist at the Department of Material Science and Engineering at MIT. Abeer also teaches a course related to empowering science in the oil and gas industry at MIT.

She holds an executive certificate on Innovation and Strategy from the MIT Sloan School of Management. Abeer also served on the Board of Directors at the American Chemical Society-Saudi Arabia section as the first female member in 2010.

She is the author of a number of publications, and has several filed patents.

In 1996, Abeer received her B.S. degree in Chemistry from King Faisal University (KFU), Dammam, Saudi Arabia. She received both her M.S. and Ph.D. degrees in Analytical Chemistry from KFU, in 2004 and 2008, respectively.

Mohammed M. Al-Rubaii

*M.S. in Petroleum Engineering,
King Fahd University of Petroleum
and Minerals*

Mohammed M. Al-Rubaii is a Drilling Engineer with the Drilling Technology Division of Saudi Aramco's Exploration and Petroleum Engineering Center – Advanced Research Center (EXPEC ARC). He joined Saudi Aramco in 2012. Since that time, Mohammed has worked on several projects regarding hole cleaning automation, formation pressures automation, rheological properties of drilling fluid automation, bit hydraulics automation, and well drilling and operations performance automation.

He has developed several automated models and methods for drilling, which has contributed to increased optimization, time, and cost-effectiveness.

Mohammed is an active member of the Society of Petroleum Engineers (SPE) where he has served

on several conferences. Mohammed has published 15 SPE papers, and initiated and co-chaired several SPE advanced technical workshop series in the region.

He is also an active member of the Dhahran Geoscience Society. Mohammed has filed 10 patent applications.

He is currently working on writing a chapter for a book entitled "Data Analytics for Drilling Process Improvement."

Mohammed received both his B.S. degree and M.S. degree in Petroleum Engineering from King Fahd University of Petroleum and Minerals (KFUPM), Dhahran, Saudi Arabia. He is currently studying for his Ph.D. degree in Petroleum Engineering at KFUPM.

Timothy E. Moellendick

*B.S. in Petroleum Engineering,
Marietta College*

Timothy E. Moellendick is the Chief Technologist for the Drilling Technology Division at Saudi Aramco's Exploration and Petroleum Engineering Center – Advanced Research Center (EXPEC ARC). Timothy is considered the industry expert in casing and liner drilling applications and engineering.

In his previous role as Director of Technology for Schlumberger, he was responsible for growing the technical and operational knowledge base used to develop, plan, and execute this technology worldwide. Timothy has also held drilling operations and engineering positions, including

Senior Drilling Engineer, Drilling Manager for North America, Senior Field Engineer/Directional Driller and Operations Coordinator for the Gulf Coast of Mexico.

With more than 25 years of oil and gas industry experience, he leads a team of world-class researchers in developing the next generation of drilling technology required by Saudi Aramco's Drilling and Workover stakeholders.

In 1996, Timothy received his B.S. degree in Petroleum Engineering from Marietta College, Marietta, OH.

Systems and Procedure for Obtaining Relative Permeability Ratio from Data Acquired during Drilling Operation

Babatope O. Kayode and Dr. Bander N. Al-Ghamdi

Abstract /

Relative permeability (k_r) is a concept introduced into Darcy's flow equation to account for multiphase flow. k_r is measured through steady-state or unsteady-state laboratory experiments, each with its peculiar advantages and disadvantages. This article discusses the basis for a new, faster, more reliable, and cost-effective methodology for acquiring relative permeability ratio (k_{rr}) data while drilling, and presents the modifications required to current flow equations to replace the use of k_r with the use of k_{rr} .

After drilling through a reservoir section, relevant logs like resistivity and porosity are acquired and interpreted for water saturation (s_w). Zones of constant average s_w are then tested using conventional drill stem test equipment, and the relative amounts of oil and water in the extracted liquid are determined at the surface using standard water cut determination procedures. Using equations derived and discussed in this article, these flow data are converted to a plot of k_{rr} as a function of average water saturation $k_{rr}(s_w)$ and saturation dependent total phase mobility $M_t(s_w)$. For the purpose of this article, an open source experimental k_r data and corresponding rock and fluid properties were used to simulate drill stem test fluid flow rates; the k_{rr} and M_t were then computed from these flow data at various averages of s_w .

Conventional steady-state and unsteady-state k_r experiments are carried out on restored cores having limited dimensions and whose initial s_w , wettability, and fluid viscosity ratio may need to be restored to representative in situ conditions using industry standard approaches. The new methodology presented acquires k_{rr} data at larger scale and at in situ conditions of initial s_w , wettability, and fluid viscosity ratio, thereby eliminating the need for core restoration.

A steady-state k_r experiment on a single core takes about 10 weeks, whereas k_{rr} acquisition on an entire pay interval can be carried out within hours. A steady-state k_r measurement does not permit the estimation of critical s_w , while the unsteady-state k_r experiment does not provide k_r data for all saturations less than the breakthrough saturation. The new methodology is designed to allow the estimation of critical s_w and residual oil saturation. These parameters are important inputs during numerical simulation tasks of history matching and field development predictions.

Introduction

Relative permeability (k_r) is the ratio of effective permeability of a phase to a reference such as its permeability when it fully saturates the porous medium. Experimental data over the years have noted multifaceted complexity associated with the direct laboratory measurement of k_r . Work by Leverett (1939)¹ and Leverette and Lewis (1941)² leads to the conclusion that k_r to a phase is only a function of the saturation of that phase. Later work by other researchers, e.g., Odeh (1959)³ and Aboujafar (2014)⁴, have shown that the k_r of the non-wetting phase is not only a function of saturation, but also a function of the fluid viscosity ratio when the sample's single-phase permeability is greater than 1 Darcy. Odeh (1959)³ claims that theoretical explanations by Yuster (1951)⁵ supports his conclusions, although several authors like Baker (1960)⁶ have criticized Odeh's findings.

It has been shown that to obtain reliable k_r measurements in the laboratory, attention must be given to address problems such as capillary end effects, hysteresis, and scaling effects⁷⁻⁹. It has also been shown that in some situations of strong oil-water preferential wettability, useful k_r measurement data can be obtained at room temperature using dead or refined oil, however, such tests may provide misleading results for mixed wettability rocks^{10,11}. In addition, it has been shown that when transporting the core from the reservoir to the surface condition, this process removes the confining stresses and potentially results in changes in the core's pore structure.

For laboratory data to be useful in scaling up to the field level, measurements should be taken at conditions representative of those found in the reservoir. This entails aging¹⁰ the core to restore the wettability state and performing the test with the appropriate combination of viscous, capillary, and gravity forces representative of reservoir conditions^{8,10}, as well as restituting the reservoir's confined pressure and stress conditions.

Steady-State k_r Measurement

Oil and water are injected simultaneously into the core at a constant rate or constant pressure for a period required to reach equilibrium. Pressure gradient, flow rates, and saturations are measured — and with the aid of Darcy's law — used to obtain an effective permeability for each phase. The key advantage of this method is the ability to determine the k_r for a wider range of saturation levels; therefore, it is the method of choice by many. Its key demerit is its inherent time requirement and necessity for an independent measurement of fluid saturation in the core.

Unsteady-State k_r Measurement

This is the fastest approach for obtaining k_r in the laboratory. It consists of displacing fluid by a constant rate or the constant pressure injection of a driving fluid and measuring the flow rate of the displaced fluids at the core's exit face. The data is then analyzed using the Buckley-Leverette equation for linear displacement of immiscible and incompressible fluids by often neglecting capillary end effects.

The limitations of the unsteady-state approach is the occurrence of viscous fingering and channeling in heterogeneous cores, and the fact that no k_r data is measured prior to injected fluid breakthrough. In addition, the operational requirement for the use of viscous oil (as a means of reducing viscous fingering of injected water) and high injection rates masks the role of capillarity and wettability. The centrifuge technique is an unsteady-state measurement believed to overcome the viscous fingering problem of unsteady-state measurement and provides the most reliable estimate of residual non-wetting phase saturation than other techniques by better simulating the gravity drainage process^{7,12}.

It is because of these limitations, difficulties, and uncertainties associated with the laboratory measurement of k_r , coupled with the fact that the most reliable tests are time-consuming — especially when it involves aging a core to its presumed original wettability (it can sometimes require about 5 weeks) — that several researchers¹³⁻¹⁵ have been motivated to explore the possibility of obtaining k_r data in situ.

Some of these approaches are based on inverse solutions^{14,15} in which k_r is derived from history matching of field data, while Al-Rushaid et al. (2017)¹³ has currently provided an approach to independently determine the k_r using downhole measured data.

Described next are some of the steps proposed¹³ and the inherent limitations of assumptions.

1. Absolute permeability is calculated from pressure transient analysis (PTA) done at free water level. Conduct another PTA at the oil zone and divide the interpreted effective oil permeability by the absolute permeability obtained in the free water level. This step already assumes that the reservoir rock is homogeneous, and therefore, the differences in effective permeability thickness (kh) between the oil zone and free water level is due only to differences in the fluid viscosity of oil and water, respectively.

This is a rarely adequate assumption. Moreover, in low permeability, reservoirs where the free water level may be significantly deeper than the dry-oil zone (large transition zone); drilling further down to free water level to conduct a baseline PTA measurement may represent a significant additional cost.

2. The k_r endpoints were determined from log interpretation. The minimum water saturation ($s_{w\min}$) on logs is used as the k_{rw} endpoint, while the lowest oil saturation is interpreted as the s_{or} . The limitation of this approach is that in reservoir rocks with sections containing significant bound water, if the lowest $s_{w\min}$ in the reservoir interval is interpreted as the k_{rw} endpoint, this would lead to significant water production from the bound water region, whereas in reality, the bound water is immobile.
3. A PTA is conducted within the transition zone and interpreted for effective oil and water permeability using the relative flow rates of each phase. These effective oil and water permeabilities are then converted to k_r by normalizing with the absolute permeability obtained from the PTA conducted below the free water level. The limitations here are as explained earlier; the absolute permeability in the transition zone is not necessarily similar to that below the free water level. Therefore, the differences in effective permeability may not be only due to fluid viscosity differences.

In this current work, we propose an alternative multiphase flow parameter that can be determined from downhole data independent of history matching and propose modifications to multiphase flow equations that would permit the use of the proposed alternative multiphase flow parameter.

Mathematical Basis for New Methodology

The original Darcy's flow equation, Eqn. 1, was derived for flow of single-phase incompressible liquid; particularly the equation was derived for use in the field of hydrology to study the flow of water in the water table.

$$q = \frac{kA\Delta P}{\mu\beta\Delta x} \quad 1$$

In oil reservoir studies, single-phase flow is an idealistic assumption; this is because the drainage process through which oil accumulates in originally water-bearing sands does not completely eliminate the connate water. This connate water flows alongside the oil — in the transition zone — during production. In addition, most reservoirs either experience aquifer support or some sort of fluid injection (gas, water, surfactants) for pressure support or improvement of sweep.

Therefore, a correction term is needed to be incorporated into Eqn. 1 to account for the reduction in the flow of the main phase in the presence of other phases within the rock pore system. This correction term is referred to as k_r , Equation 1 can therefore be re-written as:

$$q = \frac{k k_r A \Delta P}{\mu \beta \Delta x} \quad 2$$

In general, the equation for radial flow under semi-steady-state conditions is given by:

$$q = \frac{khk_r\Delta P}{141.2\mu\beta\left(\ln\frac{r_e}{r_w}-0.75\right)} \quad 3$$

The k_r is measured in the laboratory using the steady-state approach or unsteady-state approach. Once the k_{ro} and k_{rw} data have been determined as a function of s_w , the flow of each phase can be independently calculated as:

$$q_o = \frac{khk_{r_o}\Delta P}{141.2\mu_o\beta_o\left(\ln\frac{r_e}{r_w}-0.75\right)} \quad 4$$

$$q_w = \frac{khk_{r_w}\Delta P}{141.2\mu_w\beta_w\left(\ln\frac{r_e}{r_w}-0.75\right)} \quad 5$$

An expression can be derived for the produced water-oil ratio at in situ conditions by dividing Eqn. 5 with Eqn. 4 as follows:

$$\frac{q_w}{q_o} = \frac{\kappa_{rw}/\mu_w\beta_w}{\kappa_{ro}/\mu_o\beta_o} \quad 6$$

An expression for k_{rr} can be obtained from Eqn. 6 as follows:

$$\kappa_{rr} = \frac{\kappa_{rw}}{\kappa_{ro}} = \frac{q_w\mu_w\beta_w}{q_o\mu_o\beta_o} \quad 7$$

In addition, an expression for the total liquid rate can be obtained by adding Eqn. 4 and Eqn. 5 as:

$$q_t = q_o + q_w = \frac{kh\Delta P}{141.2\left(\ln\frac{r_e}{r_w}-0.75\right)} \left[\frac{\kappa_{ro}}{\mu_o\beta_o} + \frac{\kappa_{rw}}{\mu_w\beta_w} \right] \quad 8$$

We can re-write Eqn. 8 as:

$$q_t = \frac{kh\Delta P}{141.2\left(\ln\frac{r_e}{r_w}-0.75\right)} M_t \quad 9$$

$$\text{where } M_t = \left[\frac{\kappa_{ro}}{\mu_o\beta_o} + \frac{\kappa_{rw}}{\mu_w\beta_w} \right] \quad 10$$

Note that over a moderate range of pressures, total phase mobility (M_t) can be sufficiently assumed as a sole function of s_w when reservoir fluids are of low compressibility and viscosity. These assumptions are adequate for the flow of oil above bubble point pressure.

If a flow test is performed on a known interval length of a reservoir at several ΔP , Eqn. 9 suggests that a plot of q_t vs. ΔP will yield a slope R from which M_t can be determined as:

$$M_t(s_w) = \frac{141.2\left(\ln\frac{r_e}{r_w}-0.75\right)R}{kh} \quad 11$$

Where h is the flow interval and k is the average interval permeability, and r_e is the test's investigation radius. The product kh and r_e can be obtained from interpretation of the pressure transient data recorded during the mini drill stem test, Fig. 1.

From the principles of well testing¹⁶, the sequence of pressure transient behavior during partial penetration is: (1) early radial flow representing only the contribution from the perforated interval, kh , (2) spherical flow from which k_v/k can be estimated, and (3) when the diffusion has reached the upper and lower boundaries, the flow regime becomes radial again, but this time corresponding to kh . Figure 2 shows the early radial flow kh .

From the foregoing, the phase flow rates at any saturation can be computed by rearranging Eqn. 9 and

Fig. 1 A schematic of the flow regimes during a mini drill stem test.

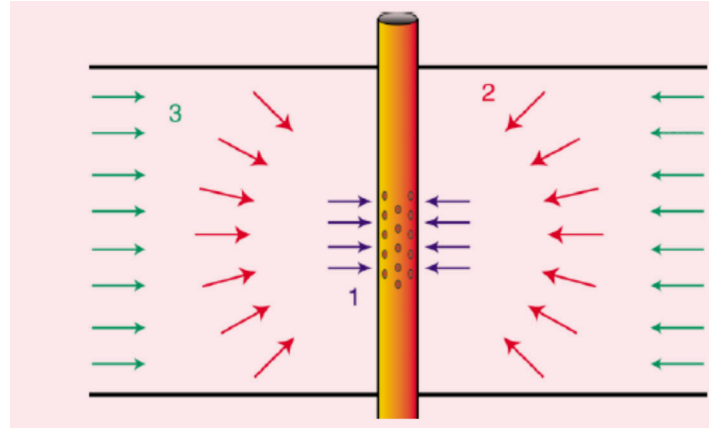
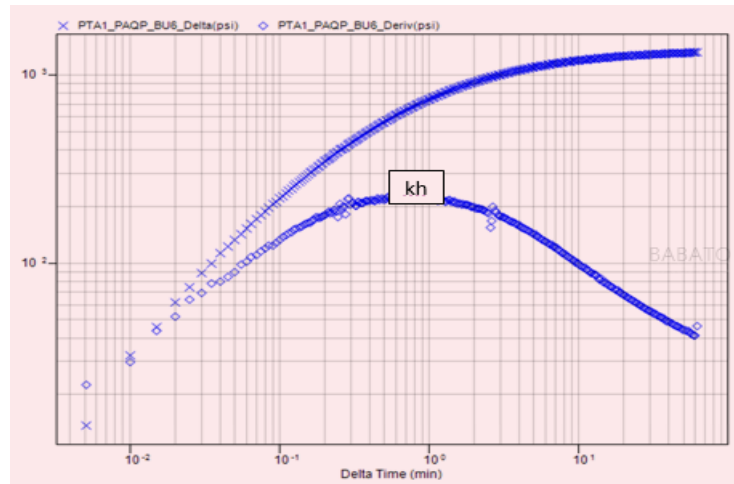


Fig. 2 The sample Log-Log diagnostic plot showing stage-1 stabilization (permeability*perforation thickness).



Eqn. 6 as follows:

$$q_t = q_o + q_w = \frac{kh\Delta P}{141.2\left(\ln\frac{r_e}{r_w}-0.75\right)} M_t \quad 12$$

$$\frac{q_w}{q_o} = \frac{\mu_o\beta_o}{\mu_w\beta_w} \kappa_{rr} \quad 13$$

Equations 12 and 13 can be solved simultaneously for each phase flow rate to obtain:

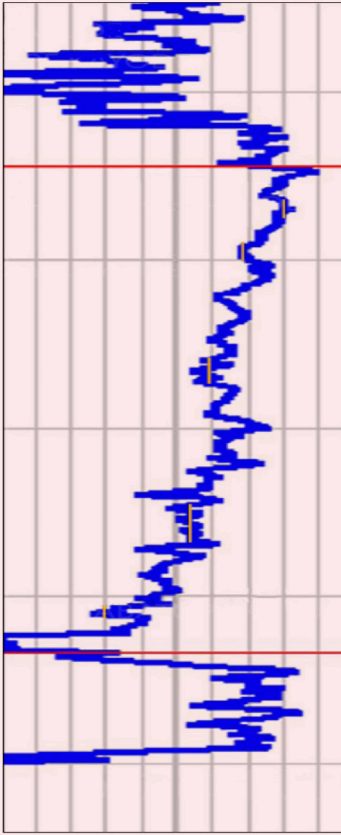
$$q_o = \frac{kh\Delta P}{141.2\left(\ln\frac{r_e}{r_w}-0.75\right)} * \frac{M_t(s_w)}{\left(1 + \frac{\mu_o\beta_o\kappa_{rr}}{\mu_w\beta_w}\right)} \quad 14$$

$$q_w = \frac{q_o\mu_o\beta_o}{\mu_w\beta_w} \kappa_{rr} \quad 15$$

Procedure for Field Application

After a well has been logged, various sections with different s_w are identified, Fig. 3, and tested as described here.

- Impose a drawdown of 100 psi over a 1 ft interval and record the stabilized oil and water flow rate, then

Fig. 3 Example of S_w log.**Table 1** Open source relative permeability data.

S_w	K_{rw}	K_{ro}
0.2	0	0.8
0.25	0.002	0.61
0.3	0.009	0.47
0.35	0.02	0.37
0.4	0.033	0.285
0.45	0.051	0.22
0.5	0.075	0.163
0.55	0.1	0.12
0.6	0.132	0.081
0.65	0.17	0.05
0.7	0.208	0.027
0.75	0.251	0.01
0.8	0.3	0

Table 2 Calculation of k_{rr} from fluid phases' rate and rock and fluid properties.

S_w	K_{rw}	K_{ro}	dP psi	Q_w bbl	Q_o bbl	K_{rr}
0.2	0	0.8	500	0	0.757654	0
0.25	0.002	0.61	500	0.024624	0.577711	0.003279
0.3	0.009	0.47	500	0.110807	0.445122	0.019149
0.35	0.02	0.37	500	0.246238	0.350415	0.054054
0.4	0.033	0.285	500	0.406292	0.269914	0.115789
0.45	0.051	0.22	500	0.627906	0.208355	0.231818
0.5	0.075	0.163	500	0.923391	0.154372	0.460123
0.55	0.1	0.12	500	1.231188	0.113648	0.833333
0.6	0.132	0.081	500	1.625169	0.076713	1.62963
0.65	0.17	0.05	500	2.09302	0.047353	3.4
0.7	0.208	0.027	500	2.560872	0.025571	7.703704
0.75	0.251	0.01	500	3.090283	0.009471	25.1
0.8	0.3	0	500	3.693565	0	—

increase the drawdown to 200 psi, 300 psi, and 500 psi, up to a maximum ΔP such that the $P_{wf} = P_b$, and measure the stabilized liquid flow rates in all cases.

- For each drawdown flow period, use Eqn. 7 to determine k_{rr} . This value should be approximately identical for all drawdown pressure values assuming that the fluids have low compressibility and low viscosity. This assumption is adequate for the flow of oil above P_b .
- From the recorded multirate pressure transients, kh and t_c can be estimated using principles of PTA, and then using Eqn. 11, the M_t is computed.
- Repeat these steps for various log saturation intervals and come up with a curve for k_{rr} vs. s_w and M_t vs. s_w .
- A plot of the interval kh vs. the interval average porosity (from density, sonic, or neutron log) from multiple wells is used for reservoir flow-type definition.
- Finally, Eqns. 14 and 15 can then be used to predict the phase flow rates at any saturation, and for any drawdown pressure.
- Any s_w interval where the maximum $\Delta P (P_i - P_b)$ produces single-phase oil is the operational critical water saturation, S_{wcr*} for the rock type and any s_w where the maximum ΔP produces single-phase water is the operational residual oil saturation, S_{or*} , for the rock type.

The S_{or*} determined from this new methodology is more operationally reliable than the S_{or} determined from laboratory experiments. This is because the S_{or*} is based on the maximum expected displacement pressure rather than the arbitrarily large displacement pressures used in determining the S_{or} in the laboratory. The S_{or*} provides a more reliable estimate of mobile oil recoverable by primary and secondary recovery mechanisms.

Also, the s_{wcr*} determined from this methodology reflects the presence of bound water. If a log section shows s_w that is higher than the lowest s_w in the reservoir interval, and if the application of maximum ΔP still does not result in water production, it simply implies such water represents bound water.

The k_r data shown in Table 1 is representative of the flow from a given reservoir Res-xyz.

Using Eqns. 4 and 5, individual phase flow rates were computed and the total flow rate calculated from the sum. A pressure drawdown of 500 psi was assumed, permeability of 10 md, flow interval of 1 ft, oil viscosity of 5 cP, water viscosity of 0.5 cP, oil formation volume factor of 1.3, and a water formation volume factor of 1.0.

Table 2 summarizes the computed flow rates, which are used to represent actual measured flow rate. Also shown is the calculated k_{rr} .

Figure 4 shows the plot of the k_{rr} vs. the s_w .

At each saturation, multirate flow tests are conducted and the results are shown in Table 3.

Figure 5 shows the plot of the total fluid rate vs. the drawdown pressure at each s_w .

The M_t is then determined from the slope of each data series using Eqn. 11.

Figure 6 shows the plot of M_t vs. s_w .

Finally, using Eqns. 14 and 15 together with the M_t and k_{rr} from the relevant plots, we can predict the phase flow rates. Table 4 shows that the predicted flow rates using the parameters k_{rr} and M_t derived in this article

Fig. 4 The calculated k_{rr} vs. s_w .

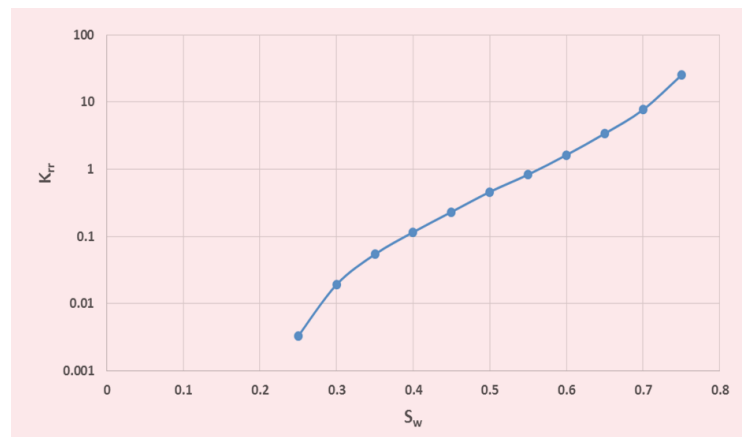


Table 3 The fluid flow rate at various drawdown pressure for different average water saturations.

$S_w = 0.2$		$S_w = 0.3$		$S_w = 0.4$		$S_w = 0.5$		$S_w = 0.6$		$S_w = 0.7$		$S_w = 0.8$	
ΔP	qt												
100	0.151531	100	0.111186	100	0.135241	100	0.215553	100	0.340376	100	0.517289	100	0.738713
200	0.303062	200	0.222372	200	0.270483	200	0.431105	200	0.680752	200	1.034577	200	1.477426
300	0.454593	300	0.333557	300	0.405724	300	0.646658	300	1.021129	300	1.551866	300	2.216139
400	0.606124	400	0.444743	400	0.540965	400	0.862211	400	1.361505	400	2.069154	400	2.954852
500	0.757654	500	0.555929	500	0.676207	500	1.077763	500	1.701881	500	2.586443	500	3.693565

Fig. 5 The total liquid rate vs. the drawdown pressure at different water saturations.

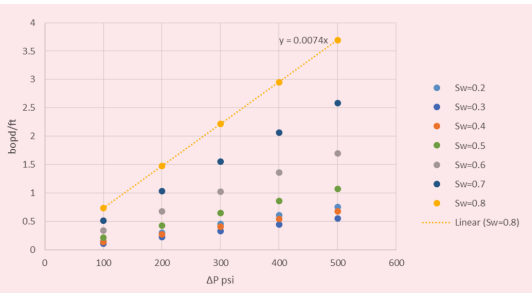


Fig. 6 The plot of M_t vs. s_w .

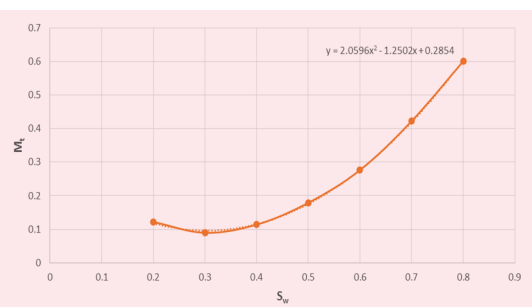


Fig. 7 The comparison plot of the calculated rate vs. the measured rate.

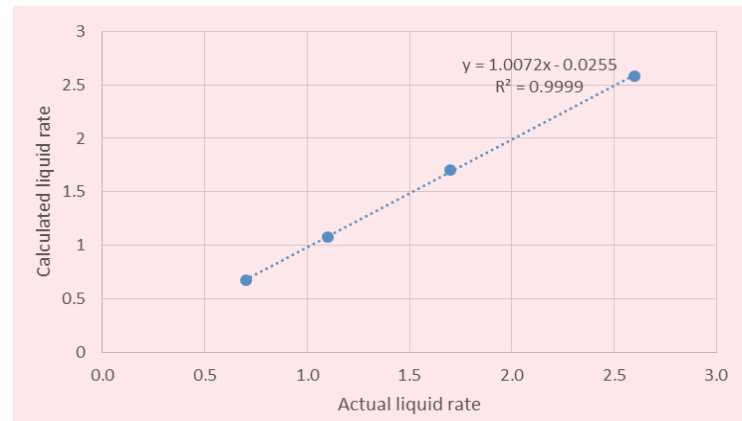


Table 4 Using values of k_{rr} and M_t at various saturations to compute phase flow rates.

S_w	K_{rr}	M_t	q_o	q_w	q_t	Measured
0.6	1.62963	0.276156	0.76628	1.623373	1.7000003	1.701881206
0.5	0.460123	0.178689	0.157557	0.942443	1.1000000	1.07776339
0.4	0.115789	0.113711	0.279412	0.420588	0.7000000	0.676206556
0.7	7.703704	0.422356	0.025705	2.574295	2.6000000	2.586442724

are very close to the actual data.

Figure 7 plots the correlation between the calculated rate and the measured rate, along with showing that the equations developed are able to effectively predict the measured rates.

Conclusions

In this article, we have developed equations and procedures for obtaining the k_{rr} from information obtained during drilling. The approach is faster than conventional steady-state and unsteady-state k_r experiments. It is more representative of in situ conditions of wettability and the viscosity ratio and provides data based on averaging larger rock volumes. Subsequently, due to the inherent assumptions, this approach cannot be used to obtain the gas-oil k_{rr} since the viscosity of gas is highly pressure dependent.

Acknowledgments

This article was prepared for presentation at the 14th Middle East Geosciences Conference and Exhibition, Manama, Kingdom of Bahrain, September 14-17, 2020.

Nomenclature

- q_o, q_w, q_t = Flow rate (oil, water, total)
- μ_o, μ_w = Viscosity (oil, water)
- β_o, β_w = Formation volume factor (oil, water)
- k_{ro}, k_{rw} = Relative permeability (oil, water)
- r_w = Wellbore radius
- r_e = Reservoir radius
- R = slope of qt vs. ΔP plot

References

- Leverett, M.C.: "Flow of Oil-Water Mixtures through Unconsolidated Sands," *Transactions of the AIME*, Vol. 132, Issue 1, December 1939, pp. 149-171.
- Leverett, M.C. and Lewis, W.B.: "Steady Flow of Gas-Oil-Water Mixtures through Unconsolidated Sands," *Transactions of the AIME*, Vol. 142, Issue 1, December 1941, pp. 107-116.
- Odeh, A.S.: "Effect of Viscosity Ratio on Relative Permeability," *Petroleum Transactions of the AIME*, Vol. 216, Issue 1, December 1959, pp. 346-353.
- Aboujafar, S.M.: "Effect of Oil Viscosity and Brine Salinity/Viscosity on Water/Oil Relative Permeability and Residual Saturations," paper presented at the SPWLA 55th Annual Logging Symposium, Abu Dhabi, UAE, May 18-22, 2014.
- Yuster, S.T.: "Theoretical Considerations of Multiphase Flow in Idealized Capillary Systems," paper WPC-4129, presented at the 3rd World Petroleum Congress, The Hague, the Netherlands, May 28-June 6, 1951.
- Baker, P.E.: "Discussion of Effect of Viscosity Ratio on Relative Permeability," *Journal of Petroleum Technology*, Vol. 12, Issue 11, November 1960, pp. 65-66.
- Heavyside, J.B., Black, C.J.J. and Berry, J.F.: "Fundamentals of Relative Permeability: Experimental and Theoretical Considerations," SPE paper 12173, presented at the SPE Annual Technical Conference and Exhibition, San Francisco, California, October 5-8, 1983.
- Honarpour, M. and Mahmood, S.M.: "Relative Permeability Measurements: An Overview," *Journal of Petroleum Technology*, Vol. 40, Issue 8, August 1988, pp. 963-966.
- Braun, E.M. and Blackwell, R.J.: "A Steady-State Technique for Measuring Oil-Water Relative Permeability Curves at Reservoir Conditions," SPE paper 10155, presented at the SPE Annual Technical Conference and Exhibition, San Antonio, Texas, October 4-7, 1981.
- Jennings Jr., H.Y.: "Effect of Laboratory Core Cleaning on Water-Oil Relative Permeability," SPE paper 897-G, presented at the Fall Meeting of the Society of Petroleum Engineers of AIME, Dallas, Texas, October 6-9, 1957.
- Hagoort, J.: "Oil Recovery by Gravity Drainage," *Society of Petroleum Engineers Journal*, Vol. 20, Issue 3, June 1980, pp. 139-150.
- Osoba, J.S., Richardson, J.G., Kerver, J.K., Hafford, J.A., et al.: "Laboratory Measurements of Relative Permeability," *Journal of Petroleum Technology*, Vol. 3, Issue 2, February 1951, pp. 47-56.
- Al-Rushaid, M., Al-Rashidi, H., Ahmad, M., Hadibeik, H., et al.: "Downhole Estimation of Relative Permeability with Integration of Formation Tester Measurements and Advanced Well Logs," paper presented at the SPWLA 58th Annual Logging Symposium, Oklahoma City, Oklahoma, June 17-21, 2017.
- Liang, L., Zhu, J., Wang, F., Chen, J., et al.: "In Situ Estimation of Relative Permeability and Capillary Pressure from the Joint Inversion of Array Resistivity and Formation Test Data," SPE paper 187193, presented at the SPE Annual Technical Conference and Exhibition, San Antonio, Texas, October 9-11, 2017.
- Zakirov, S.N., Indrupskiy, I.M., Zakirov, E.S., Anikeev, D.P., et al.: "Well Test for In Situ Determination of Oil and Water Relative Permeability," SPE paper 162011, presented at the SPE Russian Oil and Gas Exploration and Production Technical Conference and Exhibition, Moscow, Russia, October 16-18, 2012.
- Houze, O., Viturat, D. and Fjaere, O.S.: *Dynamic Data Analysis, Chapter 6, "Well Models,"* v4.12.03, KAPPA, 1988-2012.

About the Authors

Babatope O. Kayode

M.S. in Petroleum Engineering,
Heriot-Watt University

Babatope O. Kayode is a Petroleum Engineer working with the Reservoir Simulation Division in Saudi Aramco's Reservoir Description & Simulation Department.

Babatope's previous work experience with SOWSCO Well Services Nigeria Ltd. involved the planning, supervision, and interpretation of pressure transient tests.

He also worked with Total Exploration and Production in Nigeria and in France, where he was involved in the construction and live updates of dynamic simulation models before joining Saudi

Aramco in November 2014.

Babatope has 20 years of industry experience spanning Africa, Europe, and the Middle East with a research interest in the area of developing workflows for faster and better history matching. He is the author of nine technical papers and seven patents in this area.

Babatope received his B.S. degree in Petroleum Engineering from the University of Ibadan, Ibadan, Nigeria, and his M.S. degree in Petroleum Engineering from Heriot-Watt University, Edinburgh, Scotland, U.K.

Dr. Bander N. Al-Ghamdi

Ph.D. in Energy and Mineral
Engineering,
Pennsylvania State University

Dr. Bander N. Al-Ghamdi is the Division Head of the Reservoir Simulation Division of Saudi Aramco's Reservoir Description and Simulation Department. Bander's career has spanned major petroleum engineering disciplines, including drilling, production, and reservoir management. Much of his development have been focused on reservoir simulation, where he led major projects, currently in use as paramount in maximizing the potential of the company's hydrocarbon resources.

In 2019, Bander received Saudi Aramco's Excellence Award, for his leading role in the reserve certification project. During the same year, he

graduated from the company's Technical Development Program with a specialty in Compositional Modeling.

Bander is an active member of the Society of Petroleum Engineers (SPE); he served as the Chairman of the SPE-Kingdom of Saudi Arabia Section during the 2018-2019 term, and is currently serving as a Board Director.

Bander received his Ph.D. degree in Energy and Mineral Engineering with a focus on Petroleum and Natural Gas Engineering from Pennsylvania State University, State College, PA.